

# Induced Energy Gap in Finite-Sized Superconductor/Ferromagnet Hybrids

Klaus Halterman<sup>1</sup> and Mohammad Alidoust<sup>2</sup>

<sup>1</sup>*Michelson Lab, Physics Division, Naval Air Warfare Center, China Lake, California 93555, USA*

<sup>2</sup>*Department of Physics, K.N. Toosi University of Technology, Tehran 15875-4416, Iran*

(Dated: October 5, 2018)

We theoretically study self-consistent proximity effects in finite-sized systems consisting of ferromagnet (F) layers coupled to an  $s$ -wave superconductor (S). We consider both  $SF_1F_2$  and SH nanostructures, where the  $F_1F_2$  bilayers are uniformly magnetized, and the ferromagnetic H layer possesses a helical magnetization profile. We find that when the  $F_1F_2$  layers are weakly ferromagnetic, a hard gap can emerge when the relative magnetization directions are rotated from parallel to antiparallel. Moreover, the gap is most prominent when the thicknesses of  $F_1$  and  $F_2$  satisfy  $d_{F1} \leq d_{F2}$ , respectively. For the SH configuration, increasing the spatial rotation period of the exchange field can enhance the induced hard gap. Our investigations reveal that the origin of these findings can be correlated with the propagation of quasiparticles with wavevectors directed along the interface. To further clarify the source of the induced energy gap, we also examine the spatial and energy resolved density of states, as well as the spin-singlet, and spin-triplet superconducting correlations, using experimentally accessible parameter values. Our findings can be beneficial for designing magnetic hybrid structures where a tunable superconducting hard gap is needed.

PACS numbers: 74.78.Na, 74.20.-z, 74.25.Ha

## I. INTRODUCTION

Proximity effects involving superconductor (S) and ferromagnet (F) hybrid structures is of fundamental importance in the design of cryogenic spin-based devices.<sup>1-6</sup> By placing a ferromagnet and a superconductor in close contact, the mutual interactions between the two materials can result in an infusion of magnetism into the superconductor and a leakage of the superconducting correlations into the ferromagnet. Numerous recent studies of these types of systems strongly rely on the influence that proximity effects have on the superconducting and intrinsically non-superconducting elements.<sup>1-4</sup> The majority of these works explicitly assume that a finite superconducting gap or pair potential,  $\Delta$ , is present in the non-superconducting segments. For example, having a large proximity-induced gap in semiconductor nanowires with spin-orbit coupling, or in a chain of magnetic atoms attached to an  $s$ -wave superconductor, is vitally important for the experimental realization of Majorana fermions in these platforms.<sup>5-13</sup> Previous self-consistent calculations revealed that for sufficiently weak ferromagnets, there can be an induced hard superconducting gap when a single finite-sized uniformly magnetized layer is attached to a superconductor.<sup>14</sup> In more recent works, however, attention has been directed towards semiconductor wires proximity coupled to  $s$ -wave superconductors. Indeed, the presence of a sufficiently large hard gap within the semiconductor wires is an essential ingredient when hosting topological superconductivity.<sup>5,6</sup>

In a ballistic  $SF_1F_2$  or SH system, interfering quasiparticle trajectories can have a significant influence on the energy spectra, and size-effects can come into play. If an energy gap  $E_g$  exists, quasiparticles in the ferromagnetic region with energies less than  $E_g$  impinging upon the interface of the superconductor can reflect as a particle or hole with opposite charge. This Andreev reflection process can dominate other interface processes, resulting in multiple bound states and superconducting correlations inside the F layers. Due to

these proximity effects, the superconductor can subsequently induce a gap in the quasiparticle spectrum for sufficiently thin ferromagnetic layers.<sup>14</sup> For conventional bulk isotropic superconductors,  $\Delta$  is constant, and corresponds to the minimum excitation energy in the spectrum,  $E_g$ . Thus,  $E_g$  is the binding energy of a Cooper pair, and its existence affects most thermodynamic measurements. For inhomogeneous systems like the ones considered in this paper, the pair potential acquires a spatial dependence, making a correlation between  $E_g$  and  $\Delta$  nontrivial.

The interaction between ferromagnetism and superconductivity can also stimulate the creation of odd-frequency (or odd-time) spin-triplet Cooper pairs having  $m = 0, \pm 1$  spin projections on the local quantization axis.<sup>15-32</sup> The generation of these triplet correlations have a few experimental signatures, including a non-monotonic variation of the critical temperature when the magnetization vectors in  $SF_1F_2$  hybrids undergo incommensurate rotations.<sup>43-49,52-60</sup> For both the SH and  $SF_1F_2$  structures, all three triplet components can be induced simultaneously.<sup>19,33</sup> Another hallmark of spin-triplet superconducting correlations is the appearance of a peak in the density of states (DOS) at the Fermi energy.<sup>34-42</sup> It has been shown that the spin-polarized component of the triplet correlations can propagate deep within uniform magnetic layers and the corresponding peak in the DOS can arise in  $SF_1F_2$  structures with relatively strong magnetizations.<sup>35</sup> In contrast, for the nanostructures considered here that have weak ferromagnets, we find that the magnetization state can be manipulated to generate a hard gap in the energy spectra around the Fermi energy. It is therefore of interest to identify any contributions made by the induced triplet correlations towards the formation of a hard gap in SH and  $SF_1F_2$  structures.

To address conditions under which an energy gap can exist in ferromagnetic superconducting hybrid structures, we first solve the Bogoliubov-de Gennes (BdG) equations self-consistently for a  $SF_1F_2$  spin valve configuration. Our microscopic approach can account for atomic-scale phenomena

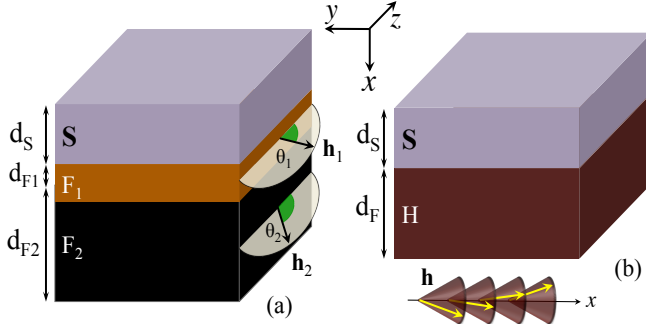


FIG. 1. (Color online). (a) Schematic of the finite size  $SF_1F_2$  trilayer, with thicknesses  $d_S$ ,  $d_{F1}$ , and  $d_{F2}$ , respectively. The magnetization,  $\mathbf{h}_{1,2}$ , in each F layer is uniform, directed in the  $yz$  plane, and constitutes angles  $\theta_{1,2}$  with the  $z$  axis. (b) We also consider a SH bilayer where H is a magnetic layer with helical magnetization  $\mathbf{h}$  that rotates on the surface of a cone when moving along the layer thickness in the  $x$  direction. The cone is characterized by a fixed apex angle of  $\alpha = 4\pi/9$ , and turning angle  $\omega$ . In both cases, (a) and (b), the interfaces are located in the  $yz$  plane.

and accommodates quasiparticle trajectories with large momenta comparable to the Fermi momenta, where quasiclassical approaches break down.<sup>35,56,58</sup> The self-consistency procedure incorporates the important step of properly accounting for the proximity effects that govern the interactions at the interfaces. We then compute the energy-resolved and spatially-resolved DOS to identify the bound states that occur in this system. Through analysis of the self-consistently found eigenvalues, we identify the location of the minimum subgap energy  $E_g$ , and show how this lowest-energy bound state evolves when varying the magnetization misalignment angle in  $SF_1F_2$  structures. We find that for a gap to be present, the F layers of the spin valve should possess *weak* exchange fields and *thin* ferromagnet layers of unequal thickness. We then reveal that the energy spectrum of the superconducting spin valve can go from gapless to gapped by simply rotating the magnetization in one of the ferromagnets. Next, we study the induction of a hard gap into a SH structure, where H is a single magnetic layer with a helical magnetization pattern. Our results show that the amplitude of the induced hard gap is enhanced by increasing the helical rotation angle, and reaches a saturation point when the magnetization cycles over a full rotation for the given thickness. By examining the spin-singlet and spin-triplet correlations, we also discuss the emergence of an energy gap with the occupation of superconducting correlations in each region of the structures.

The paper is organized as follows: In Sec. II, we briefly discuss the theoretical formalism used, and then proceed to present the main results. Specifically, we have studied the lowest-energy bound states and quasiparticle spectra, the energy and spatial resolved DOS, and the singlet and triplet superconducting pair correlations. Finally, we give concluding remarks in Sec. III.

## II. METHOD AND RESULTS

To begin, we consider the spin valve configuration shown in Fig. 1(a), where a superconductor of width  $d_S$  is adjacent to the ferromagnets  $F_1$  and  $F_2$  of widths  $d_{F1}$  and  $d_{F2}$ , respectively. For the layered spin valves considered in this work, we assume each F and S layer is infinite in the  $yz$  plane and the layer thicknesses extend along the  $x$  axis. As a result, the system is translationally invariant in the  $yz$  plane, creating an effectively quasi-one-dimensional system where any spatial variation occurs in the  $x$  direction. The corresponding BdG equations that shall be solved self-consistently are given by,

$$\begin{pmatrix} H_0 - h_z & ih_y & 0 & \Delta \\ ih_y & H_0 + h_z & \Delta & 0 \\ 0 & \Delta^* & -(H_0 - h_z) & ih_y \\ \Delta^* & 0 & ih_y & -(H_0 + h_z) \end{pmatrix} \begin{pmatrix} u_{n\uparrow} \\ u_{n\downarrow} \\ v_{n\uparrow} \\ v_{n\downarrow} \end{pmatrix} = \varepsilon_n \begin{pmatrix} u_{n\uparrow} \\ u_{n\downarrow} \\ v_{n\uparrow} \\ v_{n\downarrow} \end{pmatrix}, \quad (1)$$

where  $\varepsilon_n$  is the quasiparticle energy, the single-particle Hamiltonian is  $H_0 = -\frac{1}{2m} \frac{d^2}{dx^2} + \varepsilon_{\perp} - E_F$ , with  $E_F$  denoting the Fermi energy, and the transverse kinetic energy is defined as  $\varepsilon_{\perp} \equiv \frac{1}{2m}(k_y^2 + k_z^2)$ . The coupled set of equations in Eq. (1) are solved using an efficient numerical algorithm<sup>44</sup>, whereby the quasiparticle amplitudes  $u_{n\sigma}$  and  $v_{n\sigma}$  with spin  $\sigma(=\uparrow, \downarrow)$  are expanded in a Fourier series. The corresponding matrix eigensystem is then diagonalized, permitting the construction of all relevant physical quantities through the quasiparticle amplitudes and energies. The ferromagnets are modeled using the Stoner model with in-plane exchange fields. For the magnetization of the hybrid shown in Fig. 1(a), the ferromagnet adjacent to the superconductor,  $F_1$  has its exchange field aligned along the  $z$  direction, i.e.,  $\mathbf{h}_1 = h_0 \hat{z}$ , and for  $F_2$ , we have,

$$\mathbf{h}_2 = h_0(\sin \theta_2 \hat{y} + \cos \theta_2 \hat{z}), \quad (2)$$

where  $h_0$  is the magnitude of the exchange field, and is the same for both magnets. Thus, when  $|\theta_1 - \theta_2| \equiv \theta = 0^\circ$ , the exchange field directions are parallel, and when  $\theta = 180^\circ$ , they are antiparallel. For the magnetization profile of the SH hybrid shown in Fig. 1(b), we consider a rotating exchange field given by

$$\mathbf{h} = h_0(\cos \alpha \hat{x} + \sin \alpha[\sin(\omega x/a) \hat{y} + \cos(\omega x/a) \hat{z}]), \quad (3)$$

where the magnetization rotates on the surface of a cone with apex angle  $\alpha = 4\pi/9$ , and turning angle  $\omega$ . The quantity  $a$  corresponds to the distance of interatomic layers, which takes the normalized value  $k_F a = 2$ . Here  $k_F$  corresponds to the magnitude of the Fermi wavevector, and throughout this paper, we take  $\hbar = k_B = 1$ . Also, the energy is normalized by the bulk superconducting gap  $\Delta_0$ .

To properly account for the proximity effects that can result in a spatially inhomogenous profile for the pair potential

with strong variations near the interfaces,  $\Delta(x)$  must be self-consistently determined using a numerical algorithm. This iterative self-consistent procedure that is implemented here has been extensively discussed in previous work<sup>44</sup>. By minimizing the free energy of the system, and making use of the generalized Bogoliubov transformations<sup>61</sup>, the self-consistency equation for the pair potential is written as,

$$\Delta(x) = \frac{g(x)}{2} \sum_n' [u_{n\uparrow}(x)v_{n\downarrow}^*(x) + u_{n\downarrow}(x)v_{n\uparrow}^*(x)] \tanh\left(\frac{\varepsilon_n}{2T}\right), \quad (4)$$

where the summation over the quantum numbers  $n$  encompasses both the quantized states along  $x$ , as well as the continuum of states with transverse energies  $\varepsilon_\perp$ . Here,  $T$  is the temperature,  $g(x)$  is the attractive interaction that exists solely inside the superconducting region, and the sum is restricted to those quantum states with positive energies below an energy cutoff,  $\omega_D$ . In what follows, we define dimensionless lengths  $D_{F1} = k_F d_{F1}$ ,  $D_{F2} = k_F d_{F2}$ , and  $D_S = k_F d_S$ .

We first investigate the energy gap  $E_g$  of the spin valve as a function of the angle  $\theta$ . By applying an external magnetic field<sup>49</sup> or making use of the spin torque effect,  $\theta$  can be appropriately tuned giving the desired alignment of the magnetizations in  $F_1$  and  $F_2$ . Since the energy gap is the minimum binding energy of a Cooper pair, its existence in spin valves can play an important role in the tunneling conductance due to Andreev reflections. By tuning  $E_g$  through variations in  $\theta$ , the heat capacity and thermal conductivity of the system can also be subsequently controlled. The process of finding  $E_g$  involves calculating self-consistently the entire eigenvalue spectrum and then finding its minimum, for each angle  $\theta$ .

In Fig. 2, three panels are shown corresponding to the following exchange field magnitudes: (a)  $h_0 = 2\Delta_0$ , (b)  $h_0 = 3\Delta_0$ , and (c)  $h_0 = 4\Delta_0$ . We have found that the greatest tunable gap effect occurs when the two ferromagnets in the spin valve are relatively thin and differing in widths, with the outer ferromagnet being the largest. As the thickness of the ferromagnetic layers increases, the gap disappears. We shall discuss below the origin of our findings through investigating the dependence of the quasiparticle excitations on the transverse quasiparticle trajectories. In Fig. 2(a) five different relative widths of the ferromagnets are considered. As observed, the configuration that leads to the greatest variation in  $E_g$  is the case where  $D_{F2} = 10$  and  $D_{F1} = 5$ . Here, we see that  $\delta E_g \equiv E_g(\theta = 180^\circ) - E_g(\theta = 0^\circ) \approx 0.6\Delta_0$ . The ferromagnet directly in contact with the superconductor should be relatively thin, as it is seen that interchanging the positions of  $F_2$  and  $F_1$  results in a severe depletion of  $E_g$ . If the outer ferromagnet is reduced in size, as in the  $D_{F1} = D_{F2} = 5$  case, then the spectrum is fully gapped over the whole angular range  $\theta$ , but with a much smaller difference between the parallel and antiparallel configurations. On the other hand, increasing  $D_{F2}$  results in the destruction of the singlet pair correlations from the pair breaking effects of the magnets, and an overall reduction of the gap, as seen for  $D_{F2} = 12$ . The remaining panels in 2(b) and 2(c) present the energy gap for larger exchange fields of  $h_0 = 3\Delta_0$ , and  $h_0 = 4\Delta_0$ , with a focus on spin valve structures with optimal variations in  $E_g$ . Therefore, we

take  $D_{F1} = 5$ , and consider three different outer ferromagnet widths for each case. We again find that the best configuration is for  $D_{F2} = 10$  and  $D_{F1} = 5$ , and the gap becomes suppressed with increasing  $h_0$ . This follows from opposite-spin pair correlations experiencing greater pair-breaking effects arising from the exchange splitting of the conduction bands of the ferromagnets. We now briefly discuss the experimental observability of the proposed effect. For a superconductor with thickness  $d_S \sim 100$  nm, and  $\Delta_0 \sim 3$  meV, an energy gap opens up with  $E_g \sim 1.2$  meV, as the magnetization rotates from the parallel to antiparallel configuration. The ferromagnets in this case have exchange fields  $h_0 \sim 6$  meV, with  $d_{F2} \sim 2$  nm, and  $d_{F1} \sim 1$  nm, assuming  $k_F \sim 2\text{\AA}^{-1}$ .

We now proceed to discuss the origin of our findings by examining the quasiparticle excitation spectrum as a function of the transverse energy  $\varepsilon_\perp$ . By studying this quantity, we can reveal the quasiparticle trajectories that contribute overall to the energy gap, and the electronic spectrum can give further insight into the conditions under which a gap can exist in the spin valve structure. In Fig. 3, the energies  $\varepsilon_n$  are plotted as a function of the normalized transverse energy  $\varepsilon_\perp/E_F$ . Two different exchange field orientations are considered: (a)  $\theta = 0^\circ$ , and (b)  $\theta = 180^\circ$ . The parameters used for this case correspond to  $D_{F1} = 5$ ,  $D_{F2} = 10$ , and  $h_0 = 2\Delta_0$ . In each case a continuum of scattering states exist for  $\varepsilon/\Delta \gtrsim 1$ . In addition to this, the proximity effects arising from the mutual interaction between the ferromagnetic elements and the superconductor results in the emergence of discrete bound states. For Fig. 3(a), there is no gap in the spectrum, as it is seen that the transverse component of quasiparticle trajectories with energies close to  $E_F$  occupy low energy subgap states. As Fig. 3(b) shows, when the exchange field is rotated to the antiparallel configuration ( $\theta = 180^\circ$ ), a gap opens up, and no states are available for  $\varepsilon_n/\Delta_0 \approx 0.6$ , in agreement with Fig. 2(a). Thus, we find that “sliding” trajectories, with  $\varepsilon_\perp \approx E_F$ , play a significant role in the energy gap evolution. These states cannot be accurately described within a quasi-classical formalism.<sup>50,51</sup> The superconductor thickness is set to a representative value of  $D_S = 500$ , which permits tractable numerical solutions while retaining the general overall features. Increasing  $D_S$  would extend the reservoir of Cooper pairs to counter the ferromagnetic pair-breaking effects, resulting in only a slight increase of  $E_g$  overall. If  $D_S$  were to be made smaller, the energy gap would monotonically decline towards zero as the superconductor thickness approached the coherence length  $\xi_0$ , eventually causing the system to revert to the more energetically stable normal state.

The proximity-induced electronic density of states (DOS) can reveal signatures of the energy gap and localized Andreev bound states. One promising prospect for detecting a hard gap experimentally involves tunneling spectroscopy experiments which can probe the local single particle spectra encompassing the proximity-induced DOS. The total DOS,  $N(x, \varepsilon)$ , is the sum  $N_\uparrow(x, \varepsilon) + N_\downarrow(x, \varepsilon)$ , involving the spin-resolved lo-

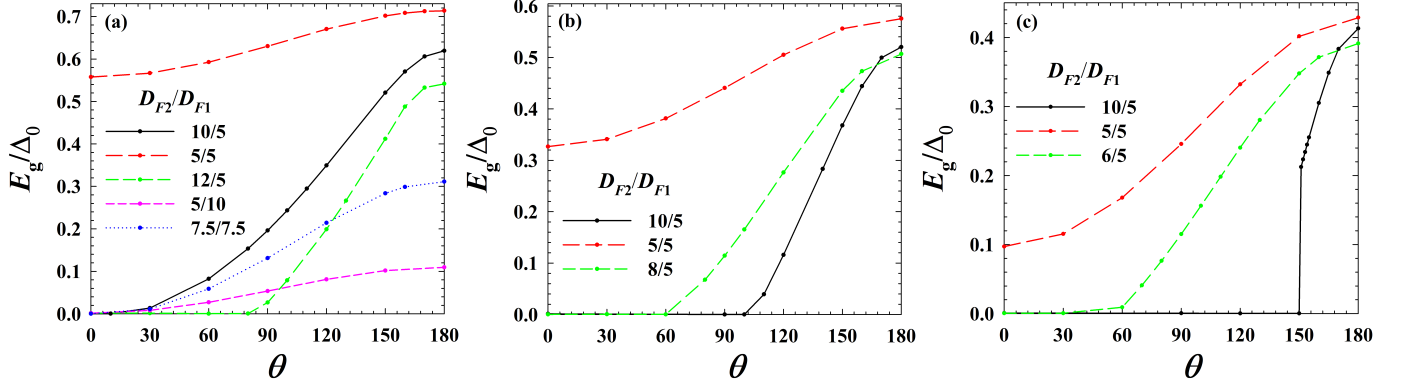


FIG. 2. (Color online). The normalized energy gap  $E_g/\Delta_0$  as a function of angle  $\theta$ , which represents the relative orientation of the exchange fields in the ferromagnets  $F_1$  and  $F_2$  for the  $SF_1F_2$  configuration. Three different exchange field strengths  $h_0$  are considered: (a)  $h_0 = 2\Delta_0$ , (b)  $h_0 = 3\Delta_0$ , and (c)  $h_0 = 4\Delta_0$ . The superconductor has normalized width  $D_S = 500$ .

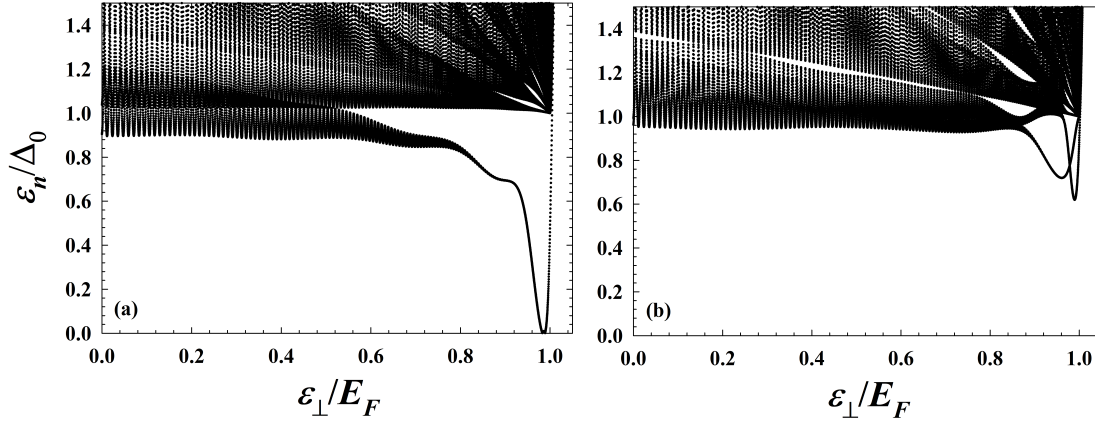


FIG. 3. (Color online). The spectral features of the  $SF_1F_2$  spin valve system. The energy eigenvalues  $\varepsilon_n$  are presented as a function of the transverse energy  $\varepsilon_\perp$ . Here,  $h_0/\Delta_0 = 2$  and  $D_S = 500$  in both panels. (a) The relative exchange field directions is parallel  $\theta = 0^\circ$ . (b) Antiparallel configuration  $\theta = 180^\circ$ .

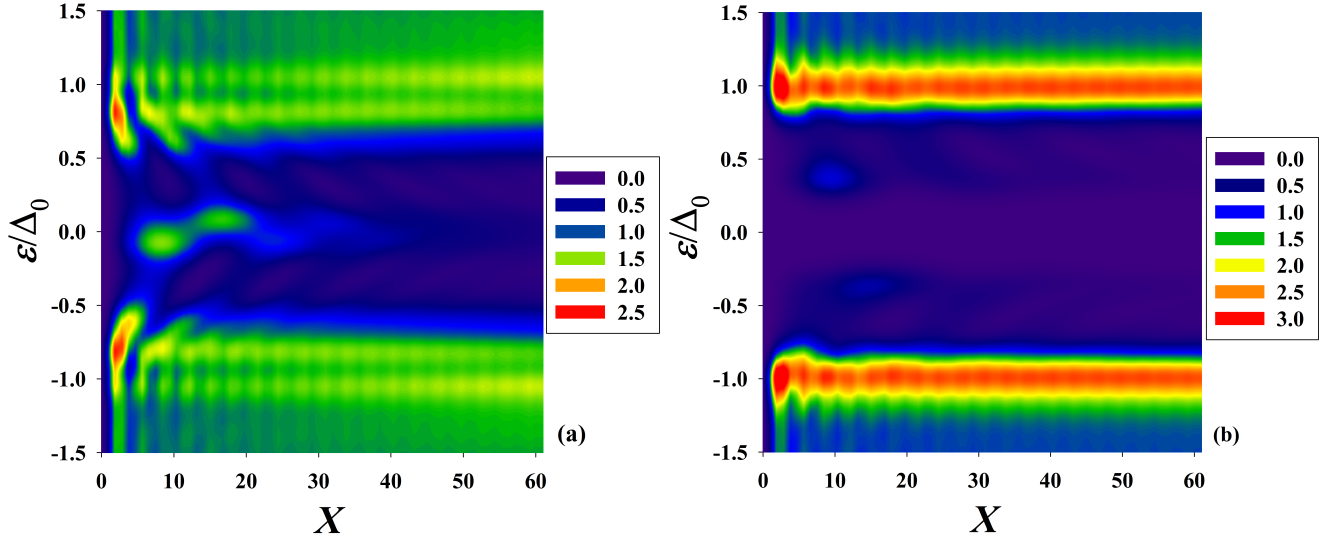


FIG. 4. (Color online). The normalized energy and spatial resolved density of states. The location within the structure is given by the normalized coordinate  $X = k_F x$ . Similar to Fig. 3 we set  $h_0 = 4\Delta_0$  and  $D_S = 500$ . In (a) the relative magnetization angle is parallel  $\theta = 0^\circ$ , while in (b) it corresponds to the antiparallel configuration  $\theta = 180^\circ$ . The interfaces are located at  $X = 6$  and  $X = 11$ .



cal DOS,  $N_\sigma$ , which are written,

$$N_\sigma = - \sum_n \{ |u_{n\sigma}(x)|^2 f'(\varepsilon - \varepsilon_n) + |v_{n\sigma}(x)|^2 f'(\varepsilon + \varepsilon_n) \}, \quad (5)$$

where  $f'(\varepsilon) = \partial f / \partial \varepsilon$  is the derivative of the Fermi function.

To investigate further how the previous results correlate with the local DOS, we show in Fig. 4 the DOS as a function of the dimensionless position  $X \equiv k_F x$ , and normalized energy  $\varepsilon / \Delta_0$ . Figure 4(a) corresponds to  $\theta = 0^\circ$ , and 4(b) is for  $\theta = 180^\circ$ . The exchange field strength in each ferromagnet is set at  $h_0 = 4\Delta_0$  and the following normalized widths are considered:  $D_{F2} = 6$ ,  $D_{F1} = 5$ , and  $D_S = 500$ . The ferromagnets thus occupy the region  $0 \leq X \leq 11$ . For the orientation  $\theta = 0^\circ$ , both exchange fields in the ferromagnets are aligned, resulting in bound states in the vicinity of zero energy within the ferromagnets and a small region of the superconductor<sup>62</sup>. Even deeper within the S region, proximity effects have resulted in the considerable leakage of subgap ( $\varepsilon < \Delta_0$ ) states that resemble traces of BCS-like peaks seen in bulk conventional superconductors. Due to the finite number of states at all energies, it can be concluded that no gap exists in the energy spectra when the magnetizations are both aligned, in agreement with Fig. 2(c). Rotating the magnetization results in the local DOS shown in Fig. 4(b). By having the exchange field directions antiparallel to one another, it is evident that there is a cancellation effect and the pair-breaking effects of the magnets become significantly weaker. The corresponding modification to the proximity effects is evidenced by the pronounced occupation of states at  $\varepsilon = \Delta_0$ . The previous bound state structure now has a few pockets of subgap states outside the energy range  $|\varepsilon / \Delta_0| \sim 0.4$ , and a complete absence of states at lower energies, consistent with Fig. 2(b), which showed  $E_g \approx 0.4$  when  $\theta = 180^\circ$ .

The broken time-reversal and translation symmetries can induce spin-triplet correlations with 0 and  $\pm 1$  spin projections along the magnetization axis. As mentioned earlier, the triplet pairs with nonzero spin projection can be revealed through single-particle signatures in the form of a DOS enhancement at low energies. To determine the precise behavior of the triplet correlations throughout the spin valve, we take the self-consistent energies and quasiparticle amplitudes calculated in Eq. (1), and perform the following sums:<sup>17</sup>

$$f_0(x, t) = \frac{1}{2} \sum_n [u_{n\uparrow}(x)v_{n\downarrow}^*(x) - u_{n\downarrow}(x)v_{n\uparrow}^*(x)] \zeta_n(t), \quad (6a)$$

$$f_1(x, t) = -\frac{1}{2} \sum_n [u_{n\uparrow}(x)v_{n\uparrow}^*(x) + u_{n\downarrow}(x)v_{n\downarrow}^*(x)] \zeta_n(t), \quad (6b)$$

$$f_2(x, t) = -\frac{1}{2} \sum_n [u_{n\uparrow}(x)v_{n\uparrow}^*(x) - u_{n\downarrow}(x)v_{n\downarrow}^*(x)] \zeta_n(t), \quad (6c)$$

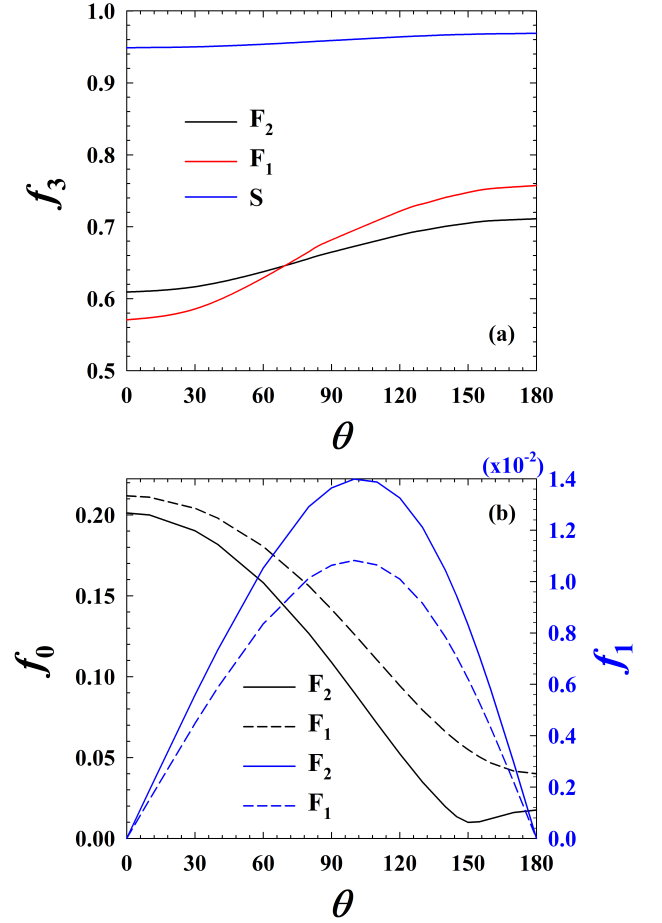


FIG. 5. (Color online). (a) The spin-singlet correlations  $f_3$ , spatially averaged over the S,  $F_1$ , and  $F_2$  layers, and plotted as a function relative of magnetization angle  $\theta$ . (b) The opposite-spin  $f_0$  and equal-spin  $f_1$  triplet pair correlations vs  $\theta$ . Here, we set  $h_0 = 4\Delta_0$ ,  $D_S = 500$ ,  $D_{F1} = 6$ , and  $D_{F2} = 5$ .

where  $f_0$  corresponds to the triplet correlations with  $m = 0$  spin projection, while  $f_1$ , and  $f_2$  have  $m = \pm 1$  spin projections. Since the spin-polarized components  $f_1$  and  $f_2$  reveal similar traits, we only present  $f_1$  below for clarity. Here  $t$  is the relative time in the Heisenberg picture, and  $\zeta_n(t) \equiv \cos(\varepsilon_n t) - i \sin(\varepsilon_n t) \tanh(\varepsilon_n / 2T)$ . The triplet amplitudes in Eqs. (6a)-(6c) pertain to a fixed quantization axis along the  $z$ -direction. When studying the triplet correlations in  $F_2$ , we align the quantization axis with the local exchange field direction, so that after rotating, the triplet amplitudes above become linear combinations of one another in the rotated system<sup>58</sup>. To describe to the proximity-induced singlet correlations beyond the S region, we must study the pair amplitude  $f_3$ , defined as  $f_3 = \Delta(x)/g(x)$ , which according to Eq. (4) yields,

$$f_3(x) = \frac{1}{2} \sum_n [u_{n\uparrow}(x)v_{n\downarrow}^*(x) + u_{n\downarrow}(x)v_{n\uparrow}^*(x)] \tanh\left(\frac{\varepsilon_n}{2T}\right), \quad (7)$$

In Fig. 5(a), the spin-singlet correlations  $f_3$  are shown spatially averaged over each of the layers in the spin valve, and plotted as a function of relative magnetization angle  $\theta$ . It is

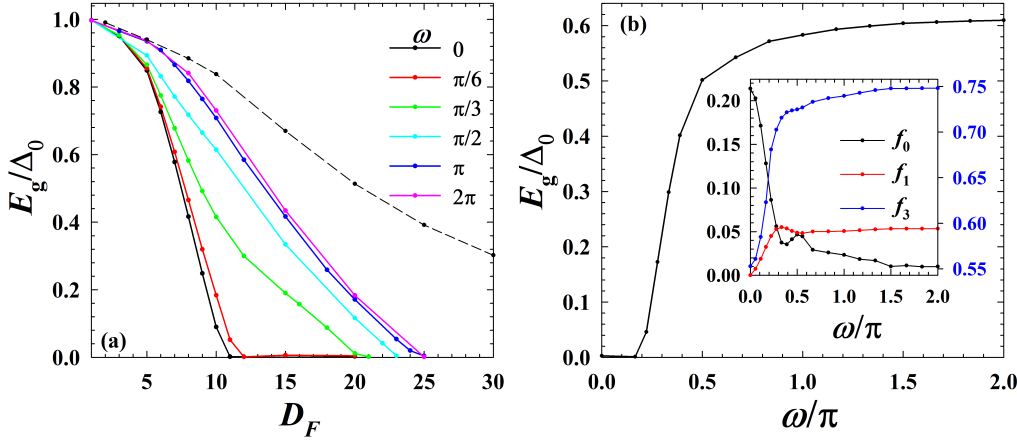


FIG. 6. (Color online). (a) The normalized energy gap  $E_g/\Delta_0$  as a function of magnetic layer thickness  $D_F$  for various rotating angle  $\theta$  of a helical magnetization. (b) The normalized energy gap vs  $\theta$  when  $D_F = 12$ . The superconductor has normalized width  $D_S = 500$ . The inset panel in (b) illustrates the behavior of spin triplet and spin singlet correlations.

evident that all regions of the structure exhibit a continual increase in singlet correlations as the magnetization rotates from the parallel to antiparallel state. These trends are consistent with the behavior of the energy gap shown in Fig. 2(c). In Fig. 5(b) we present the magnitudes of the equal-spin triplet amplitude ( $f_1$ ), and opposite-spin triplet amplitude ( $f_0$ ), each averaged over the given magnet shown in the legend. For the triplet correlations, a representative value for the normalized relative time  $\tau$  is set at  $\tau = \omega_D t = 4$ . We consider also the case  $h_0 = 4\Delta_0$ . As seen,  $f_1$  vanishes at  $\theta = 0$  and  $\theta = \pi$  since the exchange fields in each magnet are collinear with a single quantization axis. The maximum of  $f_1$  for both magnets occurs at  $\theta \approx 100^\circ$ , which corresponds to high non-collinearity between the relative exchange fields<sup>35,56</sup>. This is in contrast to the opposite-spin correlations, which are largest in the parallel configuration ( $\theta = 0^\circ$ ) and then decline rapidly towards the antiparallel state ( $\theta = 180^\circ$ ). As observed in Fig. 2(c), a gap opens up for antiparallel state, corresponding also to an enhancement of the singlet pair amplitude. Therefore, the opposite-spin singlet pair amplitude is anticorrelated to the opposite-spin triplet pair correlations as the relative exchange field orientation varies. The behavior of the triplet correlations in this figure demonstrates that the presence of zero energy states seen in Fig. 4(a) is not due to equal-spin triplet correlations, since they vanish when  $\theta = 0^\circ$ , but rather arise from singlet proximity effects, and conventional Andreev reflection between the ferromagnet and superconductor<sup>62</sup>.

To complement our investigations, we consider an alternate bilayer setup where the superconductor is now attached to a ferromagnet layer with a helical magnetization pattern, as depicted in Fig. 1(b). We show in Fig. 6(a), the energy gap variations as a function of ferromagnetic layer thickness  $D_F$ . As written in Eq. (3), the helical configuration is characterized by apex and rotating angles  $\alpha$  and  $\omega$ , respectively. The energy gap evolution for differing values of  $\omega = 0, \pi/6, \pi/3, \pi/2, \pi, 2\pi$  are shown. The case  $\omega = 2\pi$  results in the smallest slope of  $E_g$  vs  $D_F$ , and increases beyond that were found to induce no discernible changes. All curves fall beneath the nonmagnetic SN case (dashed line), shown for comparison. In order to gain additional insight on how  $E_g$  varies when  $\omega$  increases, in Fig. 6(b),  $E_g$  is plotted vs  $\omega$  for  $D_F = 12$ . It is apparent that  $E_g$  reaches a saturation limit

for large values of  $\omega$ . In other words, when  $\omega$  is sufficiently large, further increases in the rotating angle introduce only incremental variations in  $E_g$ . The inset panel in Fig. 6(b) illustrates the corresponding variations of the singlet and triplet correlations as a function of  $\omega$ . As seen, the equal-spin triplet  $f_1$  and spin singlet  $f_0$  components reach a saturation limit, identical to  $E_g$ , while the opposite-spin triplet component  $f_0$  exponentially declines and vanishes at large values of  $\theta$ .

Implementing a microscopic, self-consistent technique like the one used here is necessary to solve finite-sized spin valve structures and capture the full impact of the proximity effects. Previous works<sup>35,56</sup> that take this important approach have studied similar spin valve structures as Fig. 1(a), except that the outer magnets had either moderate exchange fields or were half-metallic. Due to the contributions from the equal-spin triplet correlations, it was shown<sup>35</sup> that by rotating the magnetization, a zero-energy peak can emerge in the DOS, ideally when  $d_{F2} > d_{F1}$  and  $\theta \sim 90^\circ$ . By using weak ferromagnets (of the order of  $\Delta_0 \sim \text{meV}$ ) that are relatively thin, we have shown here that by rotating the magnetization vector, instead of an increase in quasiparticle states at low energies, an energy gap can open up at the Fermi energy, in stark contrast to what happens when larger  $F_2$  thicknesses ( $d_{F2} \sim 400 \text{ nm}$ ) and exchange energies ( $0.1E_F \sim \text{eV}$ ) are used.<sup>35,56,58</sup> Therefore, depending on the magnetization strength and thickness of the F layers, two contrasting phenomena can arise: a controllable hard gap in the energy spectra or a zero energy peak.

### III. CONCLUSIONS

In summary, we have investigated the induction of a superconducting hard gap from a superconductor into two types of ferromagnetic structures. Particularly, we considered  $SF_1F_2$  and SH configurations where the magnetization in  $F_1$  and  $F_2$  is uniform and can possess different orientations, while H has a helical magnetization pattern. Our results demonstrated that when the thickness of the magnetic layer adjacent to the superconductor is smaller than the second layer ( $d_{F2} \geq d_{F1}$ ), a favorable situation is established for inducing a significant hard gap into the magnetic layers. Also, we found that the magnitude of the induced hard gap into the H layer is en-

hanced by increasing the rotating angle of the helical magnetization, reaching a saturation point when a full rotation occurs within a given H thickness. We also examined the spin-singlet, opposite-spin triplet, and equal-spin triplet pair correlations, showing that the induction of a hard gap into the magnetic layers is anticorrelated with the behavior of the equal spin triplet pairings. The low energy density of states for the collinear magnetic configurations of the spin valve revealed subgap signatures that cannot be attributed to the presence of equal-spin triplet pairs, but follows from the proximity effects causing a leakage of opposite-spin correlations in the ferromagnetic regions and from the geometrical effects of the thin ferromagnetic layers. Another geometrical parameter that also plays an important role is the thickness of the superconductor. Reducing  $d_S$  would dampen the amplitude of the singlet Cooper pairs, eventually causing the system to revert to a nor-

mal non-superconducting state once  $d_S$  approaches the coherence length of the superconductor. This would naturally cause a corresponding drop in the energy gap, and is related to the on-off switching and strong critical temperature variations in spin valves with thin superconducting layers.<sup>49,63</sup> We considered here  $d_S \sim 5\xi_0$ , resulting in a robust energy gap as the singlet pairs have attained their bulk properties deep within the superconductor where proximity effects near the interface have diminished.

## ACKNOWLEDGMENTS

KH is supported in part by ONR and a grant of HPC resources from the DOD HPCMP. MA is supported by Iran's National Elites Foundation (INEF).

- <sup>1</sup> C. W. J. Beenakker, *Search for Majorana fermions in superconductors*, *Ann. Rev. Cond. Matt.* **4**, 113 (2013).
- <sup>2</sup> C. Nayak, S. H. Simon, A. Stern, M. Freedman, and S. Das Sarma, *Non-Abelian anyons and topological quantum computation*, *Rev. Mod. Phys.* **80**, 1083 (2008).
- <sup>3</sup> M. G. Blamire and J. W. A. Robinson, *The interface between superconductivity and magnetism: understanding and device prospects*, *J. Phys.: Cond. Matt.* **26**, 453201 (2014).
- <sup>4</sup> M. Eschrig, *Spin-polarized supercurrents for spintronics: a review of current progress* *Rep. Prog. Phys.* **78**, 104501 (2015).
- <sup>5</sup> W. S. Cole, S. Das Sarma, and T. D. Stanescu, *Effects of large induced superconducting gap on semiconductor Majorana nanowires*, *Phys. Rev. B* **92**, 174511 (2015).
- <sup>6</sup> C.K. Chiu, W.S. Cole, S.D. Sarma, *Induced spectral gap and pairing correlations from superconducting proximity effect*, *Phys. Rev. B* **94**, 125304 (2016).
- <sup>7</sup> D. Sticlet, B. Nijholt, and A. Akhmerov, *Robustness of Majorana bound states in the short-junction limit*, *Phys. Rev. B* **95**, 115421 (2017).
- <sup>8</sup> C. R. Reeg and D. L. Maslov *Hard gap in a normal layer coupled to a superconductor*, *Phys. Rev. B* **94**, 020501(R) (2016).
- <sup>9</sup> C. Reeg, D. Loss, J. Klinovaja, *Finite-size effects in a nanowire strongly coupled to a thin superconducting shell*, *arXiv:1707.08417*.
- <sup>10</sup> O. O. Shvetsov, V. A. Kostarev, A. Kononov, V. A. Golyashov, K. A. Kokh, O. E. Tereshchenko and E. V. Deviatov, *Conductance oscillations and zero-bias anomaly in a single superconducting junction to a three-dimensional Bi2Te3 topological insulator*, *EuroPhys. Lett.* **119**, 57009 (2017).
- <sup>11</sup> M. Kjaergaard, H. J. Suominen, M. P. Nowak, A. R. Akhmerov, J. Shabani, C. J. Palmström, F. Nichele, and C. M. Marcus, *Transparent Semiconductor-Superconductor Interface and Induced Gap in an Epitaxial Heterostructure Josephson Junction*, *Phys. Rev. Applied* **7**, 034029 (2017).
- <sup>12</sup> A. Ptok, K. Rodriguez, K.J. Kapcia, *Superconducting monolayer deposited on substrate: Effects of the spin-orbit coupling induced by proximity effects*, *Phys. Rev. Materials* **2**, 024801 (2018).
- <sup>13</sup> F. J. Gomez-Ruiz, J. J. Mendoza-Arenas, F. J. Rodriguez, C. Tejedor, and L. Quiroga, *Universal two-time correlations, out-of-time-ordered correlators, and Leggett-Garg inequality violation by edge Majorana fermion qubits*, *Phys. Rev. B* **97**, 235134 (2018).
- <sup>14</sup> K. Halterman, O. T. Valls, *Energy gap of ferromagnet-superconductor bilayers*, *Physica C* **397** 151-158 (2003).
- <sup>15</sup> A.I. Buzdin, *Proximity effects in superconductor-ferromagnet heterostructures*, *Rev. Mod. Phys.* **77**, 935 (2005).
- <sup>16</sup> F.S. Bergeret, A.F. Volkov, and K.B. Efetov, *Odd triplet superconductivity and related phenomena in superconductor-ferromagnet structures*, *Rev. Mod. Phys.* **77**, 1321 (2005).
- <sup>17</sup> K. Halterman, P.H. Barsic, and O.T. Valls, *Odd Triplet Pairing in Clean Superconductor/Ferromagnet Heterostructures*, *Phys. Rev. Lett.* **99**, 127002 (2007).
- <sup>18</sup> K. Halterman, O. T. Valls, and P. H. Barsic, *Induced triplet pairing in clean s-wave superconductor/ferromagnet layered structures* *Phys. Rev. B* **77**, 174511 (2008).
- <sup>19</sup> C. T. Wu, O. T. Valls, and K. Halterman, *Proximity effects and triplet correlations in Ferromagnet/Ferromagnet/Superconductor nanostructures*, *Phys. Rev. B* **86**, 014523 (2012).
- <sup>20</sup> M. Alidoust and K. Halterman, *Proximity induced vortices and long-range triplet supercurrents in ferromagnetic Josephson junctions and spin valves*, *J. Appl. Phys.* **117**, 123906 (2015).
- <sup>21</sup> H. Chakraborti, S. Deb, R. Schott, V. Thakur, A. Chatterjee, S. Yadav, R. K. Saroj, A. Wieck, S. M. Shivaprasad, K. Das Gupta and S. Dhar, *Coherent transmission of superconducting carriers through a  $\sim 2\mu\text{m}$  polar semiconductor*, *Supercond. Sci. Technol.* **31** 085007 (2018).
- <sup>22</sup> M. Alidoust and K. Halterman, *Spontaneous edge accumulation of spin currents in finite-size two-dimensional diffusive spinorbit coupled SFS heterostructures*, *New J. Phys.* **17**, 033001 (2015).
- <sup>23</sup> M. Alidoust and K. Halterman, *Long-range spin-triplet correlations and edge spin currents in diffusive spin-orbit coupled SNS hybrids with a single spin-active interface*, *J. Phys: Cond. Matt.* **27**, 235301 (2015).
- <sup>24</sup> N. Satchell and N. O. Birge, *Supercurrent in ferromagnetic Josephson junctions with heavy metal interlayers*, *Phys. Rev. B* **97**, 214509 (2018).
- <sup>25</sup> C. Fleckenstein, N. Traverso Ziani, and B. Trauzettel, *Conductance signatures of odd-frequency superconductivity in quantum spin Hall systems using a quantum point contact*, *Phys. Rev. B* **97**, 134523 (2018).
- <sup>26</sup> J. Cayao and A. M. Black-Schaffer, *Odd-frequency superconducting pairing and subgap density of states at the edge of a two-dimensional topological insulator without magnetism*, *Phys. Rev. B* **96**, 155426 (2017).

- <sup>27</sup> C. Wang, Y. Zou, J. Song, Y.X. Li, *Andreev reflection in a Y-shaped graphene-superconductor device*, *Phys. Rev. B* **98**, 035403 (2018).
- <sup>28</sup> Z. Tao, F. J. Chen, L. Y. Zhou, B. Li, Y. C. Tao and J. Wang, *Superconductivity switch from spin-singlet to -triplet pairing in a topological superconducting junction*, *J. Phys.: Condens. Matter* **30**, 225302 (2018).
- <sup>29</sup> C. Li, L.-H. Hu, Y. Zhou and F.-C. Zhang, *Selective equal spin Andreev reflection at vortex core center in magnetic semiconductor-superconductor heterostructure*, *Scientific Reports* **8**, 7853 (2018).
- <sup>30</sup> S. Hikino and S. Yunoki, *Magnetization induced by odd-frequency spin-triplet Cooper pairs in a Josephson junction with metallic trilayers*, *Phys. Rev. B* **92**, 024512 (2015).
- <sup>31</sup> M. G. Flokstra, R. Stewart, N. Satchell, G. Burnell, H. Luetkens, T. Prokscha, A. Suter, E. Morenzoni, S. Langridge, and S.L. Lee, *Observation of Anomalous Meissner Screening in Cu/Nb and Cu/Nb/Co Thin Films*, *Phys. Rev. Lett.* **120**, 247001 (2018).
- <sup>32</sup> Y. Asano, Y. Tanaka, and A. A. Golubov, *Josephson Effect due to Odd-Frequency Pairs in Diffusive Half Metals*, *Phys. Rev. Lett.* **98**, 107002 (2007).
- <sup>33</sup> C.-T. Wu, O.T. Valls, and K. Halterman, *Phys. Rev. B* **86**, 184517 (2012).
- <sup>34</sup> S. Kawabata, Y. Asano, Y. Tanaka, and A. A. Golubov, *Robustness of Spin-Triplet Pairing and Singlet-Triplet Pairing Crossover in Superconductor/Ferromagnet Hybrids*, *J. Phys. Soc. Japan* **82**, 124702 (2013).
- <sup>35</sup> M. Alidoust, K. Halterman, and O. T. Valls, *Zero Energy Peak and Triplet Correlations in Nanoscale SFF Spin-Valves*, *Phys. Rev. B* **92**, 014508 (2015).
- <sup>36</sup> Y. Tanaka and A. A. Golubov, *Theory of the Proximity Effect in Junctions with Unconventional Superconductors*, *Phys. Rev. Lett.* **98**, 037003 (2007).
- <sup>37</sup> T. Yokoyama, Y. Tanaka, and A. A. Golubov, *Manifestation of the odd-frequency spin-triplet pairing state in diffusive ferromagnet/superconductor junctions*, *Phys. Rev. B* **75**, 134510 (2007).
- <sup>38</sup> T. Yokoyama, Y. Tanaka, and A. A. Golubov, *Resonant proximity effect in normal metal/diffusive ferromagnet/superconductor junctions*, *Phys. Rev. B* **73**, 094501 (2006).
- <sup>39</sup> L. Kuerten, C. Richter, N. Mohanta, T. Kopp, A. Kampf, J. Mannhart, and H. Boschker, *In-gap states in superconducting LaAlO<sub>3</sub>/SrTiO<sub>3</sub> interfaces observed by tunneling spectroscopy*, *Phys. Rev. B* **96**, 014513 (2017).
- <sup>40</sup> G. Koren, T. Kirzner, Y. Kalcheim, and O. Millo, *Signature of proximity-induced  $p_x + ip_y$  triplet pairing in the doped topological insulator Bi<sub>2</sub>Se<sub>3</sub> by the s-wave superconductor NbN*, *Euro-Phys. Lett.* **103**, 67010 (2013).
- <sup>41</sup> G. Koren, *Strongly suppressed proximity effect and ferromagnetism in topological insulator/ferromagnet/superconductor thin film trilayers of Bi<sub>2</sub>Se<sub>3</sub>/SrRuO<sub>3</sub>/underdoped YBa<sub>2</sub>Cu<sub>3</sub>O<sub>x</sub> : a possible new platform for Majorana nano-electronics*, *Supercond. Sci. Technol.* **31**, 075004 (2018).
- <sup>42</sup> M. Alidoust, A. Zyuzin, K. Halterman, *Pure Odd-Frequency Superconductivity at the Cores of Proximity Vortices*, *Phys. Rev. B* **95**, 045115 (2017).
- <sup>43</sup> L. R. Tagirov, *Low-field superconducting spin switch based on a superconductor/ferromagnet multilayer*, *Phys. Rev. Lett.*, **83**, 2058 (1999).
- <sup>44</sup> K. Halterman and O.T. Valls, *Proximity effects at ferromagnet-superconductor interfaces*, *Phys. Rev. B* **65**, 014509 (2001).
- <sup>45</sup> L. R. Tagirov, M. Yu. Kupriyanov, V. N. Kushnir, and A. Sidorenko, *Superconducting Triplet Proximity and Josephson Spin Valves*, *Functional Nanostructures and Metamaterials for Superconducting Spintronics*. NanoScience and Technology. Springer, Cham (2018).
- <sup>46</sup> Y.N. Proshin, Y.A. Izyumov, M.G. Khusainov, *FM/S/FM/S system as the simplest superlattice logical device with two separating recording channels*, *Physica C* **367**, 181 (2002).
- <sup>47</sup> Y.V. Fominov, A.A. Golubov, M.Y. Kupriyanov, *Triplet proximity effect in FSF trilayers*, *JETP Lett.*, **77**, 510 (2003).
- <sup>48</sup> M. Avdeev, Y. Proshin, *The Solitary Superconductivity in Dirty FFS Trilayer with Arbitrary Interfaces*, *J. Low Temp.* **185**, 453 (2016).
- <sup>49</sup> J. Zhu, I.N. Krivorotov, K. Halterman, O.T. Valls, *Angular dependence of the superconducting transition temperature in ferromagnet-superconductor-ferromagnet trilayers*, *Phys. Rev. Lett.* **105**, 207002 (2010).
- <sup>50</sup> O. Šipr and B.L. Györfy, *Andreev and normal reflections at normal metal-superconductor boundaries: Limitations of the semiclassical approximation*, *J. Low Temp. Phys.* **106**, 315 (1997).
- <sup>51</sup> O. Šipr and B.L. Györfy, *Interpretation of bound states in inhomogeneous superconductors: the role of Andreev reflection*, *J. Phys. Condens. Matter* **8**, 169 (1996).
- <sup>52</sup> P.V. Leksin, N. N. Garif'yanov, I. A. Garifullin, Ya. V. Fominov, J. Schumann, Y. Krupskaya, V. Kataev, O. G. Schmidt, and B. Büchner, *Evidence for Triplet Superconductivity in a Superconductor-Ferromagnet Spin Valve*, *Phys. Rev. Lett.* **109**, 057005 (2012).
- <sup>53</sup> V.I. Zdravkov, J. Kehrle, G. Obermeier, D. Lenk, H.-A. Krug von Nidda, C. Miller, M. Yu. Kupriyanov, A.S. Sidorenko, S. Horn, R. Tidecks, L.R. Tagirov, *Experimental observation of the triplet spin-valve effect in a superconductor-ferromagnet heterostructure*, *Phys. Rev. B* **87**, 144507 (2013).
- <sup>54</sup> E. Antropov, M. S. Kalenkov, J. Kehrle, V.I. Zdravkov, R. Morari, A. Socrovisciuc, D. Lenk, S. Horn, L.R. Tagirov, A. D. Zaikin, A.S. Sidorenko, H. Hahn, R. Tidecks, *Experimental and theoretical analysis of the upper critical field in ferromagnet-superconductor-ferromagnet trilayers*, *Supercond. Sci. Technol.* **26**, 085003 (2013).
- <sup>55</sup> M.G. Flokstra, N. Satchell, J. Kim, G. Burnell, P. J. Curran, S. J. Bending, J. F. K. Cooper, C. J. Kinane, S. Langridge, A. Isidori, N. Pugach, M. Eschrig, H. Luetkens, A. Suter, T. Prokscha, and S. L. Lee, *Remotely induced magnetism in a normal metal using a superconducting spin-valve*, *Nat. Phys.* **12**, 57 (2016).
- <sup>56</sup> K. Halterman and M. Alidoust, *Half-Metallic Superconducting Triplet Spin Valves*, *Phys. Rev. B* **94**, 064503 (2016).
- <sup>57</sup> A. Srivastava, L. A. B. Olde Olthof, A. Di Bernardo, S. Komori, M. Amado, C. Palomares-Garcia, M. Alidoust, K. Halterman, M. G. Blamire, J. W. A. Robinson, *Magnetization-control and transfer of spin-polarized Cooper pairs into a half-metal manganite*, *Phys. Rev. Applied* **8**, 044008 (2017).
- <sup>58</sup> M. Alidoust and K. Halterman, *Half-Metallic Superconducting Triplet Spin MultiValves*, *Phys. Rev. B* **97**, 064517 (2018).
- <sup>59</sup> A. A. Kamashev, P. V. Leksin, J. Schumann, V. Kataev, J. Thomas, T. Gemming, B. Büchner, and I. A. Garifullin, *Proximity effect between a superconductor and a partially spin-polarized ferromagnet: Case study of the Pb/Cu/Co<sub>2</sub>Cr<sub>1-x</sub>Fe<sub>x</sub>Al trilayer*, *Phys. Rev. B* **96**, 024512 (2017).
- <sup>60</sup> A. A. Kamashev, A. A. Validov, J. Schumann, V. Kataev, B. Büchner, Y. V. Fominov and I. A. Garifullin, *Increasing the performance of a superconducting spin valve using a Heusler alloy*, *Beilstein J. Nanotechnol.* **9**, 1764 (2018).
- <sup>61</sup> P.G. de Gennes, *Superconductivity of Metals and Alloys*, (Addison-Wesley, reading, Massachusetts, 1989).
- <sup>62</sup> S. Guron, H. Pothier, N. O. Birge, D. Esteve, and M. H. Devoret, *Superconducting Proximity Effect Probed on a Mesoscopic Length Scale*, *Phys. Rev. Lett.* **77**, 3025 (1996).



- <sup>63</sup> K. Halterman and O.T. Valls, *Nanoscale ferromagnet-superconductor-ferromagnet switches controlled by magnetization orientation*, [Phys. Rev. B \*\*72\*\*, 060514 \(R\) \(2005\)](#).